Journal of Nuclear Medicine, published on August 28, 2017 as doi:10.2967/jnumed.117.197178

Comparison of the Accuracy of FMT/CT and PET/MRI for the Assessment of Antibody Biodistribution in Squamous Cell Carcinoma Xenografts

Running title: Comparison of FMT/CT and PET/MRI

Carina Hage[1], Felix Gremse (Ph.D.)[2], Christoph M. Griessinger (Ph.D.)[3], Andreas Maurer (Ph.D.)[3], Sabrina H. L. Hoffmann[3], Franz Osl[1], Bernd J. Pichler (Ph.D.)[3], Fabian Kiessling (Ph.D.)[2], Werner Scheuer (Ph.D.)[1], Thomas Pöschinger (Ph.D.)[1]

[1]Roche Pharmaceutical Research and Early Development, Discovery Oncology, Roche Innovation Center Munich, Nonnenwald 2, 82377 Penzberg, Germany;

[2]Institute for Experimental Molecular Imaging, University Clinic and Helmholtz Institute for Experimental Molecular Imaging, RWTH Aachen University, Pauwelsstr.30, 52074 Aachen, Germany;

[3]Werner Siemens Imaging Center, Department of Preclinical Imaging and Radiopharmacy, Röntgenweg 13, 72076 Tübingen, Germany.

For correspondence or reprints contact: Carina Hage, Roche Pharmaceutical Research and Early Development, Discovery Oncology, Roche Innovation Center Munich, Nonnenwald 2, 82377 Penzberg, Germany.

Phone: +4988566012001

E-mail: carina.hage@roche.com

Word Count: 5203 words

Funding information: This study was sponsored by Roche Diagnostics GmbH.

#

ABSTRACT

Non-invasive imaging technologies are increasingly used in preclinical drug research for the pharmacokinetic analysis of therapeutic compounds in living animals over time. The different preclinical imaging modalities available differ intrinsically in their detection principle and thus might exhibit limitations for a specific application. Here, we systematically investigated the performance of advanced fluorescence mediated tomography/micro-computed tomography (FMT/CT) in comparison to positron emission tomography/magnetic resonance imaging (PET/MRI) for quantitative analysis of the biodistribution of different antibody formats and in dependence of the required imaging label in squamous cell carcinoma xenografts.

Methods: Different formats of an antibody (mAb, $F(ab')_2$ and Fab) targeting epidermal growth factor receptor (EGFR) were labeled with Alexa750 or [^{64}Cu]NODAGA and injected intravenously into separate cohorts of nude mice bearing subcutaneous A-431 tumors. Two and 24 h after injection, mice were measured by FMT/CT and PET/MRI. Probe accumulation was quantitatively assessed in organs and tumors. *In vivo* data were compared between modalities and correlated with *ex vivo* fluorescence, gamma counting and electro-chemiluminescence immunoassay.

Results: Both imaging methods faithfully monitored the biodistribution and elimination routes of the compounds and organs' accumulation measured by FMT/CT and PET/MRI correlated significantly with *ex vivo* measurements. In addition, the accumulation in kidney, muscle and tumor tissue correlated between FMT/CT and PET/MRI. However, the pharmacokinetic of the Alexa750-labeled antibody formats showed shorter blood half-life times and higher liver uptake than the radiolabeled counterparts.

Conclusion: FMT/CT imaging allows quantifying the biodistribution of antibodies in nude mice and provides an alternative to PET analysis in preclinical drug research. However, even for large molecules, such as mAb, Alexa750-labeling can change pharmacokinetics and trigger liver uptake.

Keywords: PET/MRI, FMT/CT, Optical Imaging, Animal Imaging, Biodistribution

INTRODUCTION

The investigation of the biodistribution of therapeutic compounds is an integral part in preclinical drug research. The *in vivo* behavior of a biotherapeutic is dependent on many factors, such as size and charge of the molecules [1]. To investigate the biodistribution over time, animals typically have to be sacrificed for organ take at different time points, which requires a large number of animals. The clearance rate of a therapeutic compound is usually assessed by blood analysis.

With the advent of *in vivo* imaging technologies, non-invasive tracking of therapeutic compounds throughout the body became feasible [2]. Among such, PET and Single-photon emission computed tomography (SPECT) have been established as tool of choice for monitoring biodistribution. These technologies are based on detection of gamma radiation, yield high sensitivity and allow longitudinal measurements with absolute quantification [3]. The combination of PET with CT or MRI allows whole-body biodistribution imaging with anatomical information [4, 5]. However, PET imaging has some disadvantages as the use of radioisotopes is necessary, which requires high technical skills and appropriate safety measures.

In contrast, optical imaging is based on light in the visible or near-infrared range and frequently employs fluorescence dyes to obtain tissue specific information [6]. FMT is a laser-based three-dimensional (3D) optical imaging technique using multiple diffuse trans-illuminations to determine the fluorescence signals non-invasively in small animals. This technique requires fluorescence labeling which needs to be considered during pharmacokinetic analyses. Fluorescence measurements for multiple laser injection points are used to reconstruct the 3D biodistribution in the living animal which

involves complex numerical algorithms [7]. In this context, absorption and scattering parameters have to be taken into account for a correct reconstruction.

Since its introduction in 2002, FMT is characterized by an extensive application in drug development [8,9]. However, unlike PET measurements, optical imaging is strongly affected by tissue depth and tissue-specific optical properties, such as absorption and scattering. The combination with an anatomical high resolution imaging modality, e.g. CT, enables improved optical modeling [10]. A 3D scattering map can be derived from an automated segmentation in combination with tissue-dependent scattering coefficients [11]. Similar to attenuation correction in PET, an optical absorption map, derived from the FMT trans-illumination data, is used to correct for strongly absorbing organs [11]. The fusion with 3D anatomical CT datasets enables accurate positioning of the fluorescence information as described in previous work [12,13].

Despite increasing interest in optical imaging methods for preclinical drug research, there is, to our knowledge, no comprehensive data available that investigates the performance of advanced FMT/CT against PET/MRI for the quantitative assessment of drug biodistribution. Therefore, these modalities were compared using Alexa750 dye as fluorescence label and [^{64}Cu]NODAGA as radiolabel. Hence, our goal was to investigate whether FMT/CT is capable of reliably quantifying the spatial and temporal biodistribution of therapeutics and to compare its performance with PET/MRI and ECLIA analyses to distinguish imaging and labeling based effects on the FMT/CT measurements.

MATERIALS AND METHODS

Animal Experiments and Study Design

All animal studies were approved by the local government and mice were handled according to committed guidelines (Federation for Laboratory Animal Science Associations (FELASA)). Eight weeks old female athymic nude mice (Charles River, Wilmington, MA, USA) with a body weight of 22-25 g were used. Two equally designed studies were carried out for FMT/CT and PET/MRI, respectively. A-431 cells expressing EGFR (7.5×10^6 cells in 100 µL PBS) were injected subcutaneously into the right flank. At a tumor size of ~100 mm^3, mice were separated into two cohorts for FMT/CT and PET/MRI. Both cohorts were randomized into three groups (n=5) for anti-EGFR formats mAb, $F(ab')_2$ and Fab. Labeled compounds were administered by intravenous (i.v.) tail vein injection in equimolar amounts, i.e. 2 mg/kg anti-EGFR-mAb, 1.33 mg/kg anti-EGFR-$F(ab')_2$ and 0.67 mg/kg anti-EGFR-Fab, respectively.

Labeling of Antibody Formats

For FMT/CT, antibody formats were labeled with Alexa750 (SAIVI™ Rapid Antibody Labeling Kit). For PET/MRI, antibody formats were conjugated with a chelator via NHS ester chemistry and radiolabeled with ^{64}Cu as described previously [14]. More information is provided in the supplemental material (available at http://jnm.snmjournals.org).

FMT/CT Imaging

#

FMT/CT imaging was performed as described in [12]. Briefly, mice were imaged two and 24 hours after compound injection subsequently in a micro-CT (TomoScope Synergy Twin, CT Imaging GmbH, Erlangen, Germany) and a FMT scanner (FMT 2500, Perkin Elmer, Waltham, USA). Before imaging, animals were anesthetized with 2% isoflurane at 2 L/min oxygen and placed on a multimodal imaging cassette. For CT scans a high resolution protocol with 1440 projections and a scan time of 180 s was used. Both tubes were operated at 50 kV and 0.8 mA. Image reconstruction was performed using a cone-beam Feldkamp algorithm with an isotropic voxel size of 35 µm and a T50 reconstruction kernel. For FMT, around 100 laser injection points were used with 3 mm distance using the 745 nm channel. FMT and CT datasets were fused and fluorescence was reconstructed using heterogeneous absorption and scattering maps [11]. Based on CT data, various regions (liver, kidneys, leg muscle and tumor) were interactively segmented using the Imalytics Preclinical software, resulting in a binary mask for each region [15]. Fluorescence amount of each region was computed by summing the voxel intensities of all segmented voxels. Concentrations were computed by dividing the sum by the volume of the region. The required scale factors were determined using FMT/CT phantom scans with known amounts of probe for mAb, $F(ab')_2$ and Fab (Supplemental materials).

PET/MRI

For PET/MRI, mice were anesthetized (2% isoflurane at 2 L/min oxygen) and scanned for ten minutes on a small animal PET-Scanner (Inveon, Siemens Preclinical Solutions, Knoxville, USA) after two and 24 hours. Subsequently, mice were transferred to a 7T

BioSpec MRI scanner (Bruker BioSpin MRI, Ettlingen, Germany). MR imaging was performed using a whole body coil and a T2-weighted 3D TurboRARE sequence (repetition time = 1800 ms; echo time = 66.7 ms; resolution = 0.3 mm; averages = 2). PET data were reconstructed with a 2D Ordered-subset expectation maximization algorithm (matrix 128x128; voxel size 0.79x0.79 mm²) in Inveon Acquisition Workplace v. 1.5.0.28 (Siemens). PET and MRI scans were co-registered and all PET scans were normalized according to the residual activity at the beginning of the respective scan. Different regions (tumor, liver, kidney and leg muscle tissue) were segmented.

Blood Sampling and Necropsy

Blood samples were taken from the retro-orbital sinus of the left mouse eye. Mice were sacrificed and tissues (liver, kidneys, muscle and tumor) were harvested.

2D FRI

Fluorescence signal of explanted tissues of the FMT/CT study was measured by the 2D Fluorescence Reflectance Imaging (FRI) system (Maestro, Perkin Elmer). Whole organ and tumor samples were measured and mean fluorescence signals were shown as counts per second.

γ-Counting

Harvested tissues of the PET/MRI study were measured in a γ-Counter (Perkin Elmer). The samples were weighed to calculate the %ID per gram tissue.

ECLIA Analysis

ECLIA was performed to quantify the antibody amounts in tissue homogenates and blood. Chemiluminescent emission signal was induced by a voltage in the measuring cell of the Elecsys® (Cobas, E411, Roche, Penzberg, Germany) and signal was detected by a photomultiplier at 620 nm. Further information about tissue homogenization and ECLIA is provided in the supplemental materials.

Statistical Analysis

For statistical analysis GraphPad Prism6 (San Diego, CA, USA) was used. Results were expressed as mean values ± standard deviation (SD). Differences between groups were tested for significance using the one-way analysis of variance (ANOVA) followed by a Tukey multiple comparison test. $P<0.05$ was assumed to indicate significant differences. For correlation analysis, Pearson's correlation analysis was performed. Scatterplots were generated and the coefficient of correlation R^2 was determined for the mean values of each treatment group.

#

RESULTS

Evaluation of Pharmacokinetics

For side-by-side comparison of FMT/CT with PET/MRI, two equally designed *in vivo* imaging studies were performed and analyzed measuring the drug uptake in several organs and the tumor of nude mice. Prior to the *in vivo* biodistribution study of anti-EGFR drug uptake, preliminary experiments confirming anti-EGFR antibody binding as well as FMT phantom experiments as proof-of-concept were performed (see Supplemental Figure 1 and 2).

In Vivo Biodistribution after 2 h

FMT/CT imaging after two hours (Fig. 1A) showed a strong signal (>35 %ID/cm³) of all three Alexa750-labeled antibody formats in the liver of the mice and no significant differences were found between mAb, $F(ab')_2$ and Fab. In contrast, accumulation in the kidneys was strongly dependent on the size of the different antibody formats. After two hours only 7.9 %ID/cm³ of the intact mAb was found in the kidneys, while a compound level of 22.9 %ID/cm³ of $F(ab')_2$ and 52.7 %ID/cm³ of Fab was detected. The segmented muscle tissue showed only weak uptake of anti-EGFR compounds. In the tumor, accumulation was observed for all antibody formats but no significant differences were found between the formats after two hours.

PET/MRI measurements were performed analogously to the FMT/CT study in order to compare the biodistribution patterns monitored by two different technologies. As observed in the FMT/CT study, the quantitative analysis after two hours post injection

by PET/MRI showed a size-dependent clearance of the antibodies by the kidneys (mAb:F(ab')$_2$:Fab = 5.6:30.4:64.2 %ID/cm³) (Fig. 1B). However, compared to the fluorescence-labeled compounds used in the FMT/CT study, the level of radiolabeled anti-EGFR-F(ab')$_2$ and -Fab in the kidneys was higher (F(ab')$_2$-Alexa750:F(ab')$_2$-[^{64}Cu]NODAGA = 22.9:30.4 %ID/cm³ and Fab-Alexa750:Fab-[^{64}Cu]NODAGA = 52.7:64.2 %ID/cm³). In contrast, the [^{64}Cu]NODAGA-labeled constructs showed a substantially lower accumulation in the liver tissue (Fig 1B) compared to the Alexa750-labeled compounds (Fig 1A). Only low compound levels were detected in the segmented muscle tissues by PET/MRI. The tumor uptake of [^{64}Cu]NODAGA-labeled compounds was low after two hours (Fig 1B). A direct comparison of the quantitative mean values of %ID/cm³ tissue with standard deviations measured by both technologies after two hours is shown in Supplemental Table 1.

In Vivo Biodistribution after 24 h

The drug distribution determined by FMT/CT 24 hours post injection (p.i.) (Fig 2A) showed a lower level of mAb-Alexa750, F(ab')$_2$-Alexa750 and Fab-Alexa750 in the liver compared to the values after two hours (Fig 1A). The decreased level of F(ab')$_2$-Alexa750 and Fab-Alexa750 in the kidneys after 24 hours indicated an excretion of these constructs through the renal route. The strongest accumulation in the tumor was detected for mAb with 13.1 %ID/cm³. The %ID/cm³ of the fragments in the tumor tissue were significantly lower compared to the intact mAb (3.6 %ID/cm³ for F(ab')$_2$ ($p<0.01$) and 1.9 %ID/cm³ for Fab ($p<0.001$)).

The [^{64}Cu]NODAGA-labeled compounds showed a substantially lower accumulation in the liver tissue (Fig. 2B) compared to the Alexa750-labeled compounds (Fig 2A). Only

low compound levels were detected in the segmented muscle tissues by PET/MRI which is in line with FMT/CT measurement data. The tumor uptake of [^{64}Cu]NODAGA-labeled compounds increased over time indicating the highest uptake of mAb with 7.3 %ID/cm³ after 24 hours (Fig 2B). The format-dependent tumor uptake after 24 hours agreed well with the uptake of Alexa750-labeled constructs measured by FMT/CT (Fig 2A). A direct comparison of the quantitative values of %ID/cm³ tissue (mean+/-SD) measured by both technologies after 24 hours is shown in Supplemental Table 2. In order to report the signal-to-noise ratio of the *in vivo* measurements, the tumor uptake-to-muscle ratio was calculated. This is shown for both *in vivo* imaging technologies (see Supplemental Figure 3).

Correlation Analysis of FMT/CT with PET/MRI

In order to compare the results generated by PET/MRI with the FMT/CT technology, a correlation analysis was performed. An overall good correlation of FMT/CT with PET/MRI data in tumor, kidney and muscle tissues after two and 24 hours post injection of antibody formats was observed ($R^2 = 0.85$) (Fig. 3). Please note that the mean values of the livers at both time points were not included due to label-dependent differences between Alexa750 and [^{64}Cu]NODAGA in the liver uptake.

***Ex Vivo* Quantification of Compound Accumulation in Whole Organs and Tumors**

For validation of *in vivo* FMT/CT and PET/MRI, 2D FRI and *γ*-counting measurements of explanted tissues (liver, kidneys, muscle, tumor) were performed. Overall, the *ex vivo* fluorescence measurements as well as *γ*-counting showed a very good agreement with

#

FMT/CT and PET/MRI data, respectively, at two hours and 24 hours (Fig. 4). In line with the *in vivo* experiments, Alexa750-labeled compounds measured by 2D FRI indicated a substantially higher relative accumulation in the liver as compared to radiolabeled compounds quantified by *γ*-counting that also appeared independent from the antibody format. In contrast, signal levels obtained from the kidneys showed clear size-dependent compound elimination for both 2D FRI and *γ*-counting measurements as higher levels of smaller fragments were detected in the kidneys after two hours compared to the full antibody mAb. Both *ex vivo* modalities confirmed a significantly higher drug uptake in the tumor tissue for the intact mAb after 24 hours as for the fragments.

Ex Vivo Quantification of Compound Accumulation in Tissue Homogenates

ECLIA measurements were performed to quantify the amount of antibody formats present in tissue homogenates. In contrast to FMT/CT and PET/MRI, ECLIA is specific for the κ light chain of the antibody and is thereby independent of the label. ECLIA measurement at two hours confirmed a higher amount of Alexa750-labeled antibodies in the liver (25-40 %ID/cm³) (Fig. 5A) as compared to [^{64}Cu]NODAGA- labeled compounds (3-9 %ID/cm³) (Fig. 5B). In the kidneys, ECLIA confirmed the strong size-dependent accumulation for both fluorescence- and radiolabeled compounds. Antibody levels found at two hours in the tumor and muscle were low. At 24 hours antibody levels could only be detected for the intact antibody, whereas protein levels of the fragments were below the limit of quantification. In this context mAb levels in the tumor were comparable for both labels.

#

Correlation Analysis of *In Vivo* Imaging and *Ex Vivo* Technologies

A correlation analysis for *in vivo* imaging technologies with *ex vivo* ECLIA was performed. As shown in Figure 6A and B a strong correlation was found between the *in vivo* biodistribution data at two hours post injection of FMT/CT and PET/MRI with the ECLIA values in the liver, kidney, muscle and tumor tissues (R^2 = 0.9 and 0.95, respectively).

Evaluation of Pharmacokinetics by Blood Serum Analysis

Quantification of blood serum samples at different time points (5 min, 30 min, 2 h and 24 h post injection) via ECLIA provided information about the drug clearance (Fig. 7). The Alexa750-labeled compounds (Fig. 7A) and the radiolabeled compounds (Fig. 7B) showed similar courses of blood clearance. However, blood half-life times of Alexa750-labeled compounds were slightly shorter compared to [^{64}Cu]NODAGA-labeled compounds. After 12.8 hours half of the mAb-Alexa750 was eliminated from blood whereas it took 17.2 hours for mAb-[^{64}Cu]NODAGA. The blood half-life times for the F(ab')$_2$ fragments were 1.2 hours for the fluorescence-labeled F(ab')$_2$ and 1.4 hours for the radiolabeled F(ab')$_2$. The smaller Fab fragments showed comparable values of blood half-life times ($T_{1/2}$ (Fab-Alexa750) = 0.3 h and $T_{1/2}$ Fab-[^{64}Cu]NODAGA) = 0.3 h).

#

DISCUSSION

In this study we investigated the performance of advanced FMT/CT against PET/MRI to non-invasively and quantitatively assess the drug biodistribution of labeled therapeutic antibody formats in a preclinical cancer mouse model. For this purpose, we injected fluorescence labeled compounds and monitored organ and tumor uptake at different time points via FMT/CT. The same experiment was performed with radiolabeled compounds by using PET/MRI. Direct comparison of FMT/CT with PET/MRI and additional *ex vivo* technologies provided an adequate validation of the optical imaging technology.

Prior to clinical application the *in vivo* pharmacokinetics of therapeutic molecules need to be extensively studied. As invasive *ex vivo* methods, such as blood sampling and necropsy, require a high number of animals and do not allow longitudinal measurements, non-invasive imaging technologies are of high interest in preclinical research. PET and SPECT combined with CT and MRI are widely accepted as the gold standard for the absolute quantification of drug levels *in vivo*. The PET technology is characterized by high sensitivity and good tissue penetration properties [16]. However, Compton scattering [17] and the partial volume effect in PET imaging due to its limited spatial resolution can lead to a lack of precision [18].

This is the reason for differences between *in vivo* quantification and *ex vivo* gamma counting results. In addition, the radiation exposure and the half-life time of radioactive isotopes have to be considered. In contrast to usage of radiolabels for PET, the FMT technology requires fluorescence labeling [2]. However, light emitted by fluorescent probes is prone to strong optical absorption and scattering limiting the application to

nude mouse models or mouse hair removal if quantitative data are desired. For clinical application the usage of advanced FMT/CT is restricted to imaging of body parts that are only several centimeters away from the entry point of the light [19]. Thus, in translational theranostic studies, PET might be more appropriate [20].

In our study, FMT/CT and PET/MRI data correlate with *ex vivo* measurements and show similar biodistribution patterns when comparing them with each other. In addition, except for liver, *in vivo* imaging data of different labeled compounds, measured with both modalities, correlated well, qualifying FMT/CT for routine preclinical drug research with nude mice. The difference in the liver uptake was not expected, but may result from the label characteristics, such as hydrophobicity and charge. The immunoreactivity of the protein after the labeling procedure is important to know prior to *in vivo* application. For our imaging experiments we demonstrate proper binding of labeled antibody to A-431 tumor cells by microscopy analysis. However, we recommend the performance of further binding affinity studies (e.g. Biacore) for future experiments. Only few studies investigated the altered protein characteristics after labeling and reported that Alexa750- labeling increases the liver uptake [21]. The altered liver concentration was described to be a result of the number of fluorescent dye molecules per compound as well as from the conformation of the labeled substance [22]. Therefore, protein to dye ratio particularly needs to be considered as the degree of labeling may affect the biodistribution. In addition, Ho et al. showed that the indocyanine green dye (ICG) accumulated in the liver and was transcytosed by hepatocytes via the transporter organic anion transport protein (OATP) [23]. Hence, the similarity of Alexa750 to ICG may cause liver uptake through the same transporter. Apart from that, radiocopper

complexes are discussed to vary in their stability [24]. Studies demonstrated that labeling a molecule with copper chelators has an influence on its liver metabolism as copper dissociates from the chelator. The dissociated Cu(II) binds to a protein called superoxide dismutase which is especially abundant in the liver [25]. Consequently, further research in the use of fluorescence and radiolabels is clearly warranted as published previously by Cilliers, Nessler et al. [26] and the label degradation *in vivo* has to be considered. The *ex vivo* ECLIA analysis is a good alternative and measures protein concentrations independent of the label. However, upon internalization of the antibody construct in the cell, the compound is presented to lysosomes, is cleared within the cell and cannot be detected anymore via ECLIA analysis.

Furthermore, our consecutive FMT/CT as well as PET/MRI measurements proved that the intact antibody showed the highest uptake in the tumor accompanied by a long persistence in the blood. The $F(ab')_2$ and Fab fragments showed a lower tumor uptake as they were rapidly cleared through the renal route resulting in low bioavailability in serum. The short blood half-life time of the fragments presumably diminishes the penetration of the fragments to the tumor tissue. The clearance kinetics of the different antibody formats shown in this study match with a former study focusing on the kinetics of a specific mAb and fragments for prostate cancer demonstrating the faster blood clearance of antibody fragments compared to complete antibodies [27]. In general, fragments diffuse easier from the circulating blood and are eliminated faster by the kidney compared to intact antibodies [28]. Overall, both technologies, FMT/CT and PET/MRI, provided valid data of the drug biodistribution in kidney, muscle and tumor tissues.

#

CONCLUSION

To the best of our knowledge, this study addresses for the first time the detailed side-by-side evaluation of the performance of small animal FMT/CT with PET/MRI for preclinical evaluation of drug distribution. The strong correlation of the FMT/CT and PET/MRI measurements with the *ex vivo* results as well as the consistency of the biodistribution patterns determined by both *in vivo* technologies qualifies advanced FMT/CT as a convenient and cost-effective technology to obtain pharmacokinetic information of therapeutic compounds in nude mice and as a promising alternative to classical PET. However, the influence of the fluorescence label has to be carefully considered as it may change the liver uptake and thus, could lead to wrong conclusions on drugs' biodistribution.

DISCLOSURE

This study was sponsored by Roche. Carina Hage, Franz Osl, Werner Scheuer and Thomas Poeschinger are employees of Roche. Felix Gremse is founder of Gremse-IT GmbH. F. Gremse and F. Kiessling received funding by the German Higher Education Ministry (BMBF, Biophotonics, 13N13355) and the European Union (FP7). Bernd J. Pichler receives research support from Mediso and Roche. No other potential conflict of interest relevant to this article was reported.

#

ACKNOWLEDGMENTS

The authors wish to express their gratitude to A. Wessner for fluorescence labeling of anti-EGFR compounds as well as Klaus Mackeben and Kay-Gunnar Stubenrauch for ECLIA quantification.

References

1. Schrag M, Regal K. Pharmacokinetics and Toxicokinetics. In: A comprehensive guide to toxicology in preclinical drug development animal models in toxicology. *Academic Press*. 2013;3rd ed.:51-54.

2. Shi Y, Kunjachan S, Wu Z, et al. Fluorophore labeling of core-crosslinked polymeric micelles for multimodal in vivo and ex vivo optical imaging. *Nanomedicine (Lond)*. 2015;10(7):1111-25.

3. Griessinger CM, Kehlbach R, Bukala D, et al. In vivo tracking of Th1 cells by PET reveals quantitative and temporal distribution and specific homing in lymphatic tissue. *J Nucl Med*. 2014;55(2):301-7.

4. Bailey DL, Pichler BJ, Guckel B, et al. Combined PET/MRI: from status quo to status go. Summary report of the fifth international workshop on PET/MR imaging. *Mol Imaging Biol*. 2016;18(5):637-50.

5. Disselhorst JA, Bezrukov I, Kolb A, Parl C, Pichler BJ. Principles of PET/MR imaging. *J Nucl Med*. 2014;55(Supplement 2):2s-10s.

6. Graves EE, Weissleder R, Ntziachristos V. Fluorescence molecular imaging of small animal tumor models. *Curr Mol Med*. 2004. 4(4): p. 419-30.

7. Kunjachan S, Gremse F, Theek B, et al. Noninvasive optical imaging of nanomedicine biodistribution. *ACS Nano*. 2013;7(1):252-62.

8. Ntziachristos V, Bremer C, Weissleder R. Fluorescence imaging with near-infrared light: new technological advances that enable in vivo molecular imaging. *Eur Radiol*. 2003;13(1):195-208.

#

9. Theek B, Gremse F, Kunjachan S, et al. Characterizing EPR-mediated passive drug targeting using contrast-enhanced functional ultrasound imaging. *J Control Release*. 2014;182:83-9.

10. Ale A, Ermolayev V, Herzog E, et al. FMT-XCT: in vivo animal studies with hybrid fluorescence molecular tomography-X-ray computed tomography. *Nat Methods*. 2012;9(6):615-20.

11. Gremse F, Theek B, Kunjachan S, et al. Absorption reconstruction improves biodistribution assessment of fluorescent nanoprobes using hybrid fluorescence-mediated tomography. *Theranostics*. 2014;4(10):960-71.

12. Gremse F, Doleschel D, Zafarnia S, et al. Hybrid μCT-FMT imaging and image analysis. *J Vis Exp*. 2015;100:e52770.

13. Rosenhain S, Rawashdeh W, Kiessling F, Gremse F. Sensitivity and accuracy of hybrid fluorescence-mediated tomography in deep tissue regions. *J Biophotonics.* 2016;10:1-9.

14. Griessinger CM, Maurer A, Kesenheimer C, et al. 64Cu antibody-targeting of the T-cell receptor and subsequent internalization enables in vivo tracking of lymphocytes by PET. *Proc Natl Acad Sci USA*. 2015;112(4):1161-6.

15. Gremse F, Stärk M, Ehling J, Menzel JR, Lammers T, Kiessling F. Imalytics preclinical: interactive analysis of biomedical volume data. *Theranostics*. 2016;6(3):328-41.

16. Nanni C, Di Leo K, Tonelli R, et al. FDG small animal PET permits early detection of malignant cells in a xenograft murine model. *Eur J Nucl Med Mol Imaging*. 2007;34(5):755-62.

#

17. Mannheim JG, Judenhofer MS, Schmid A, et al. Quantification accuracy and partial volume effect in dependence of the attenuation correction of a state-of-the-art small animal PET scanner. *Phys Med Biol*. 2012;57(12):3981-93.

18. Skretting A. 'Intensity diffusion' is a better description than 'partial volume effect'. *Eur J Nucl Med Mol Imaging*. 2009;36(3):536-7.

19. Stuker, F, Ripoll J., Rudin M. Fluorescence molecular tomography: principles and potential for pharmaceutical research. *Pharmaceutics.* 2011;3(2):229-274.

20. Wehrl HF, Wiehr S, Divine MR, Gatidis S, Gullberg GT, Maier FC. Preclinical and translational PET/MR imaging. *J Nucl Med*. 2014;55(Supplement 2):11s-18s.

21. Peterson NC, Wilson GG, Huang Q, Dimasi N, Sachsenmeier KF. Biodistribution analyses of a near-infrared, fluorescently labeled, bispecific monoclonal antibody using optical imaging. *Comp Med*. 2016;66(2):90-9.

22. Cohen R, Stammes MA, de Roos IH, Stigter-van Walsum M, Visser GW, van Dongen GA. Inert coupling of IRDye800CW to monoclonal antibodies for clinical optical imaging of tumor targets. *EJNMMI Res*. 2011;1(1):31.

23. Ho CM, Dhawan A, Hughes RD, et al. Use of indocyanine green for functional assessment of human hepatocytes for transplantation. *Asian J Surg*. 2012;35(1):9-15.

24. Boswell CA, Sun X, Niu W, et al. Comparative in vivo stability of copper-64-labeled cross-bridged and conventional tetraazamacrocyclic complexes. *J Med Chem*. 2004;47(6):1465-74.

25. Bass LA, Wang M, Welch MJ, Anderson CJ. In vivo transchelation of copper-64 from TETA-octreotide to superoxide dismutase in rat liver. *Bioconjug Chem.* 2000;11(4):527-32.

#

26. #Cilliers, C., Nessler I, Christodolu N, Thurber GM. Tracking antibody distribution with near-infrared fluorescent dyes: impact of dye structure and degree of labeling on plasma clearance. *Molecular Pharmaceutics*. 2017;14(5):1623-1633.

27. Alt K, Wiehr S, Ehrlichmann W, et al. High-resolution animal PET imaging of prostate cancer xenografts with three different 64Cu-labeled antibodies against native cell-adherent PSMA. *Prostate.* 2010;70(13):1413-21.

28. Chames P, Van Regenmortel M, Weiss E, Baty D. Therapeutic antibodies: successes, limitations and hopes for the future. *Br J Pharmacol*. 2009;157(2):220-33.

#

FIGURES

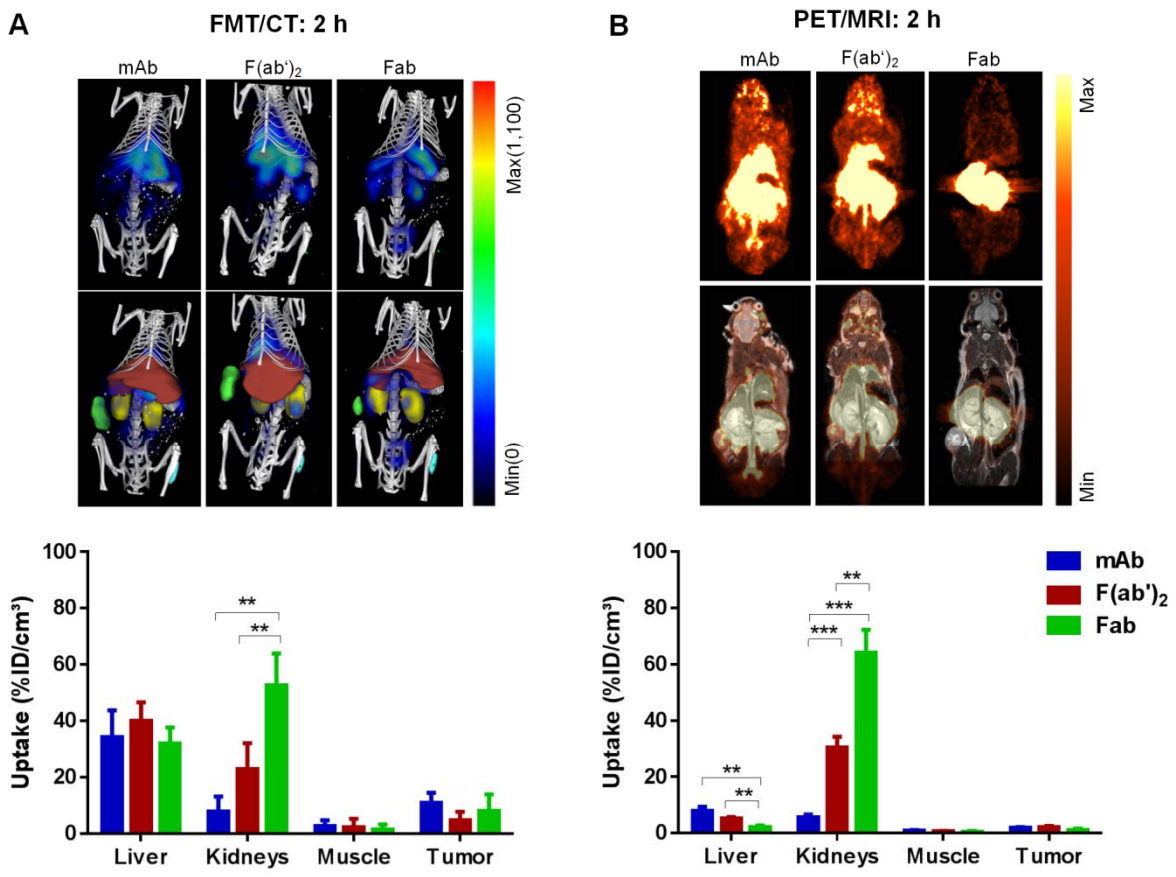

FIGURE 1: FMT/CT and PET/MRI analysis two hours post injection of anti-EGFR compounds (mAb, F(ab')$_2$, Fab). **A** Exemplary FMT images overlaid with the CT bone structure (first row) and with segmented organs (second row) illustrate the biodistribution of anti-EGFR-constructs after two hours. Segmented liver is shown in red, kidneys in yellow, muscle in cyan and tumor in green. Quantitative results of compound accumulation determined by FMT/CT is shown in a bar chart. **B** Anatomically corresponding sections of PET scans (first row) and overlay with MRI scans (second row). Quantitative results of compound accumulation determined by PET/MRI is shown in a bar chart (*p<0.05, **p<0.01, ***p<0.001).

#

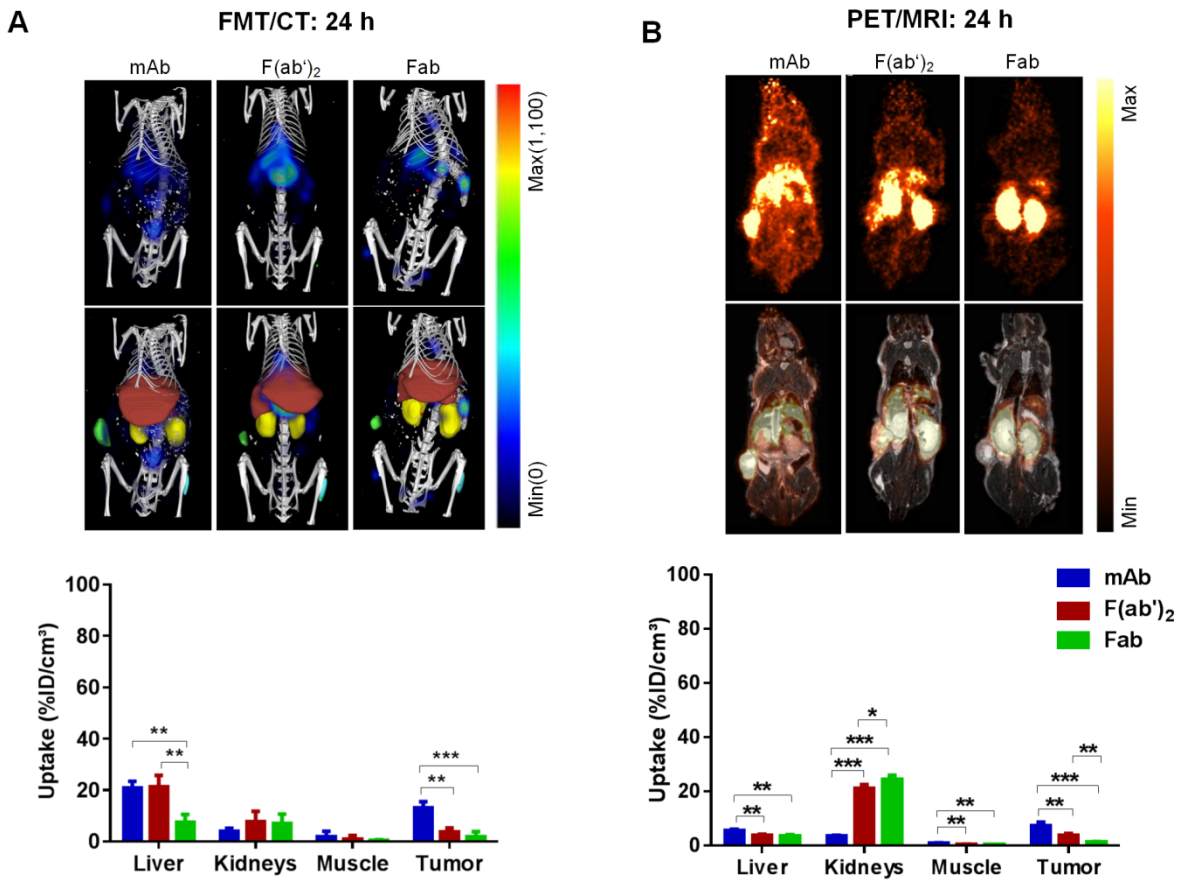

FIGURE 2: FMT/CT and PET/MRI analysis 24 hours post injection of anti-EGFR compounds (mAb, F(ab')$_2$, Fab). **A** Exemplary FMT images overlaid with the CT bone structure (first row) and with segmented organs (second row) illustrate the biodistribution of anti-EGFR-constructs after 24 hours. Segmented liver is shown in red, kidneys in yellow, muscle in cyan and tumor in green. Quantitative results of compound accumulation determined by FMT/CT is shown in a bar chart. **B** Anatomically corresponding sections of PET scans (first row) and overlay with MRI scans (second row). Quantitative results of compound accumulation determined by PET/MRI is shown in a bar chart (*p<0.05, **p<0.01, ***p<0.001).

#

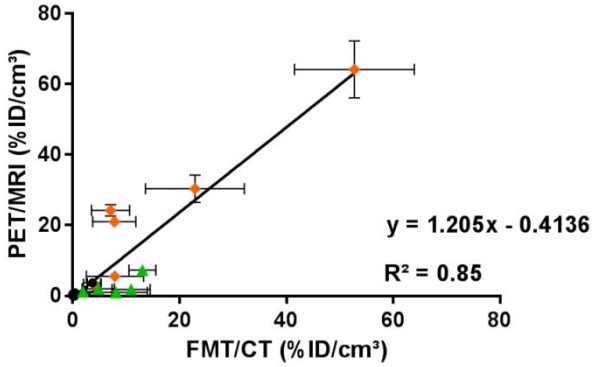

FIGURE 3: Correlation between the mean values over all animals of each group between FMT/CT and PET/MRI in different tissues (kidneys, muscles, tumors) after two and 24 hours ($p<0.0001$). Mean values of liver tissues were excluded due to differences in the uptake of the two labels.

#

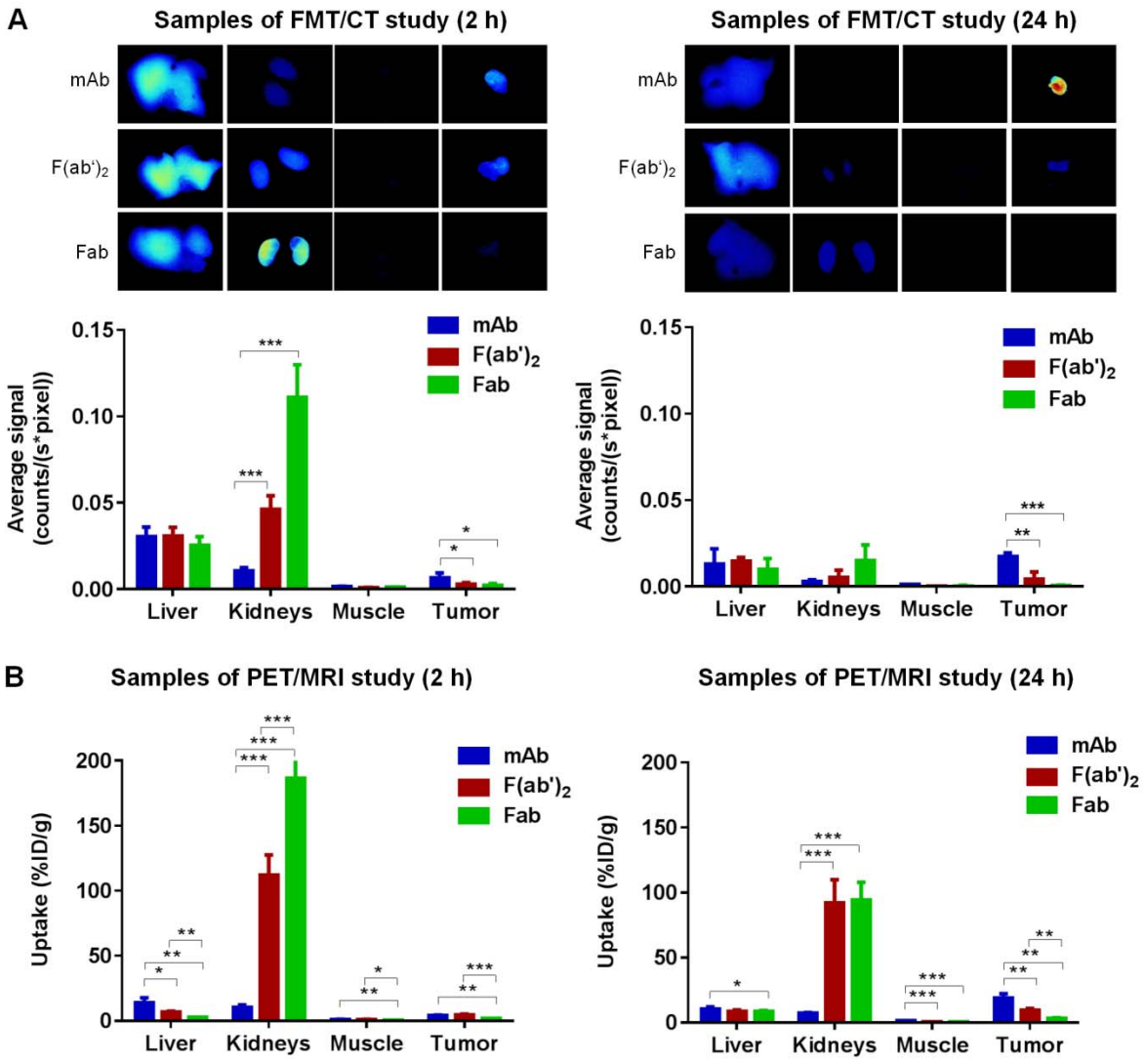

FIGURE 4: *Ex vivo* assessment of drug biodistribution after two and 24 hours post injection obtained from 2D planar fluorescence reflectance measurements (**A**) and *γ*-counting measurements (**B**) of explanted liver, kidney, muscle and tumor tissues (*p<0.05, **p<0.01, ***p<0.001).

#

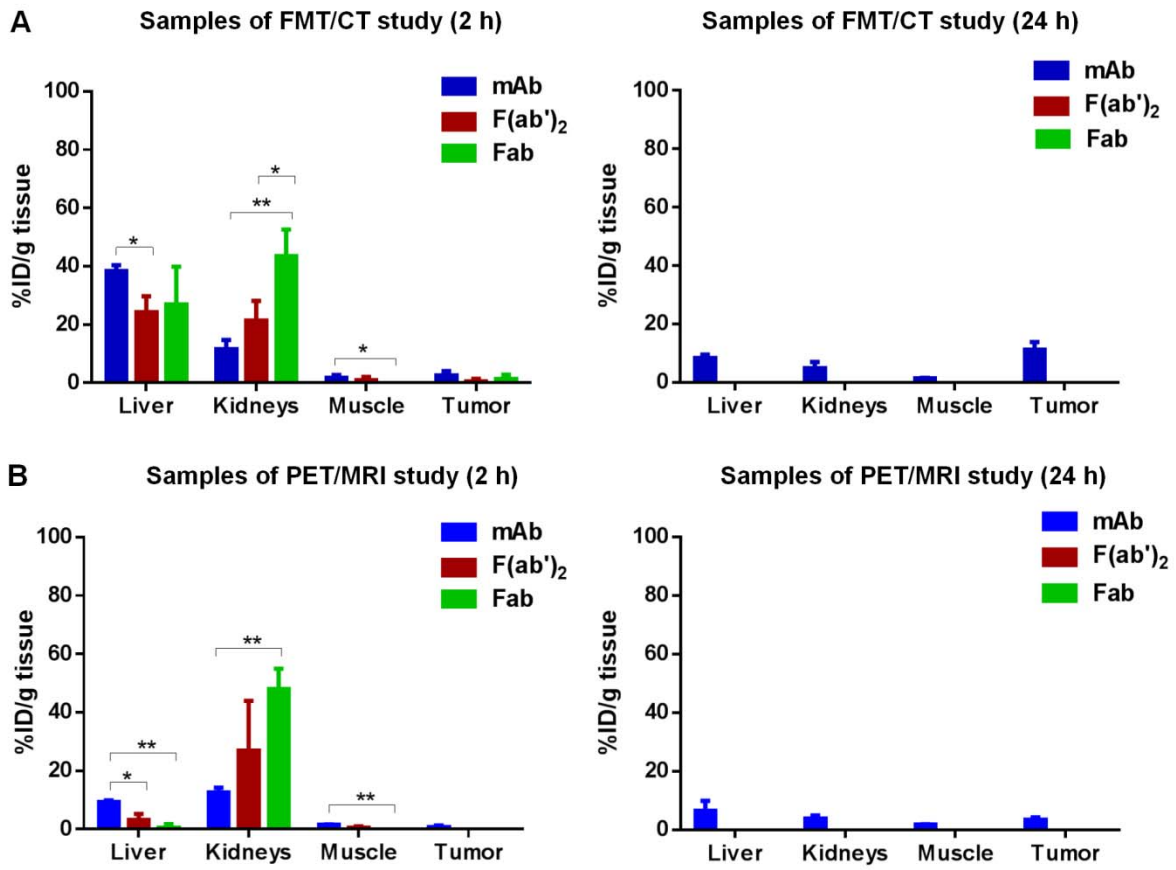

FIGURE 5: Quantification of anti-EGFR construct levels in tissue homogenates.

A Percentage injected dose of the Alexa750-labeled compounds (anti-EGFR-mAb, -F(ab')$_2$, -Fab) per gram tissue (liver, kidneys, muscle, tumor) (n=5) determined by ECLIA in tissue homogenates two hours and 24 hours post injection. **B** Percentage injected dose of the [^{64}Cu]NODAGA-labeled compounds (anti-EGFR-mAb, -F(ab')$_2$, -Fab) per gram tissue (liver, kidneys, muscle, tumor) (n=4) determined by ECLIA in tissue homogenates after two hours and 24 hours post injection (*p<0.05, **p<0.01, ***p<0.001). Please note that some levels of F(ab')$_2$ and Fab constructs were below the limit of quantification.

#

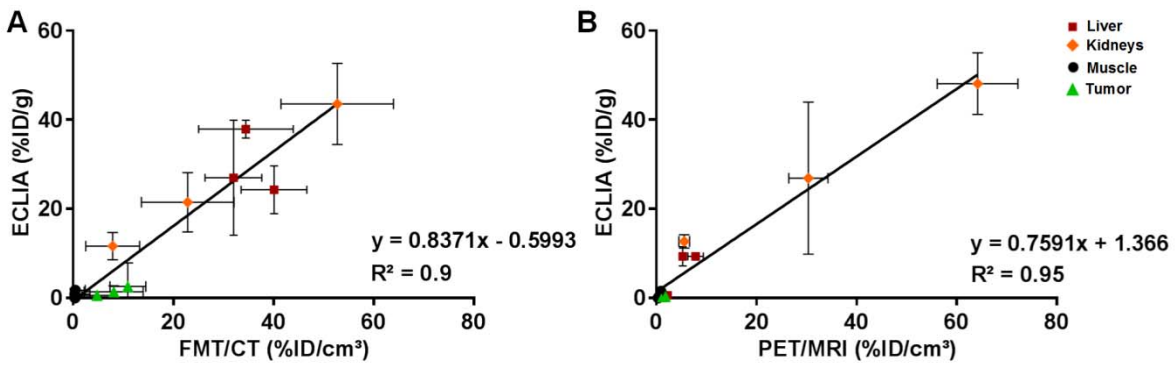

FIGURE 6: Correlation between *in vivo* and *ex vivo* biodistribution analysis.

A Correlation of the mean values over all animals of each group between FMT/CT values and ECLIA values in livers, kidneys, muscles and tumors after two hours ($p<0.0001$). **B** Correlation of the mean values over all animals of each group between PET/MRI and ECLIA values in livers, kidneys, muscles and tumors after two hours ($p<0.0001$). Each point represents one region (liver, kidneys, muscle and tumor) and one of the three antibody formats.

#

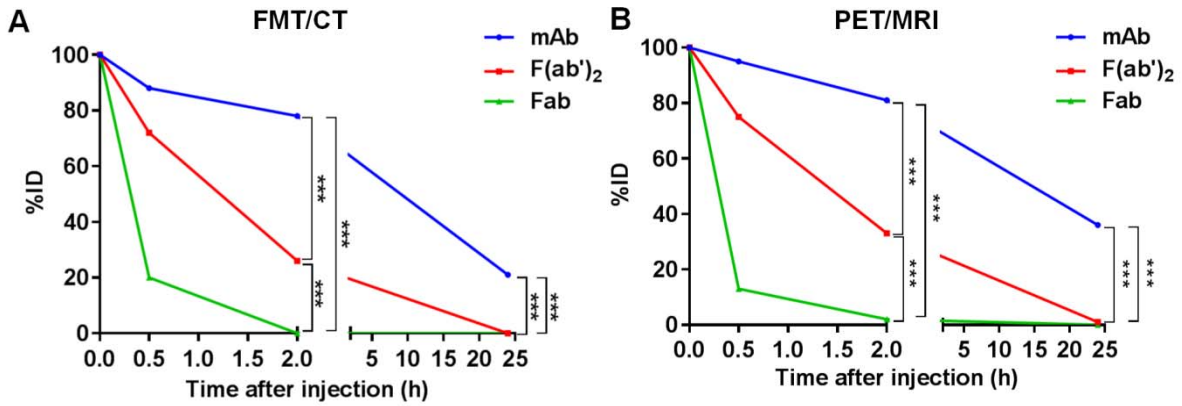

FIGURE 7: Compound level of fluorescent and radiolabeled anti-EGFR constructs in blood serum. **A** Percentage injected dose of the Alexa750-labeled compounds in blood serum samples collected at several time points (5 min, 30 min, 2 h and 24 h post injection) and quantified by ECLIA analysis (n=5). **B** Percentage injected dose of the [^{64}Cu]NODAGA-labeled compounds in blood serum samples collected at several time points (5 min, 30 min, 2 h and 24 h post injection) and quantified by ECLIA analysis (n=4) (*p<0.05, **p<0.01, ***p<0.001).

#

SUPPLEMENTAL

SUPPLEMENTAL MATERIALS AND METHODS

Labeling of Antibody Formats

For FMT/CT, antibody formats were labeled with Alexa750 (SAIVI™ Rapid Antibody Labeling Kit). The compounds were transferred to the reaction vials containing the lyophilized Alexa Fluor® dye and incubated for one hour in the dark (protein:dye conjugation ratio for mAb=1:5, for $F(ab')_2$=1:4 and Fab=1:3). During the labeling process the reactive N-hydroxysuccinimide (NHS) ester group of the fluorochrome reacts with the amines of the compound molecule to yield stable amide bonds. After the conjugation, the fluorescent conjugate was purified by size-exclusion chromatography. The protein:Alexa750dye ratio for mAb was 1:3.46, for $F(ab')_2$ was 1:2.56 and for Fab was 1:2.44.

For PET/MRI, antibody formats were conjugated with a chelator via NHS ester chemistry. Bifunctional chelator NODAGA-NHS (Chematech, Dijon, France) was added to the antibody at a molar ratio of 55:1 and incubated at 4°C for 24 h. Excess of chelator was removed by repeated ultrafiltration with 0.25 M sodium acetate (pH 6). The constructs were radiolabeled with ^{64}Cu as described previously [14] with the same molar excess for all formats, typically resulting in 3-4 chelator moieties per protein. The ^{64}Cu solution was buffered to pH 6 using 0.5 M ammonium acetate and the NODAGA-conjugated antibody was added at a ratio of 2 µg/MBq. After incubation for 1 h at 42°C, the incorporation of the ^{64}Cu was analyzed by thin layer chromatography (Agilent iTLC-SG, 0.5 M sodium citrate pH 5) and high performance size exclusion chromatography (Phenomenex BioSep-SEC-s3000, saline sodium citrate) [14].

Tissue Homogenization

Specimens were homogenized and 100 mg of each sample was solved in 1 mL lysis buffer (10 mM Tris, 137 mM NaCl, 1% Triton, 10% Glycin supplemented with protease inhibitor).

ECLIA Analysis

ECLIA was performed to quantify the antibody amounts in tissue homogenates and blood. A volume of 65 µL of a biotin-labeled capture antibody (IgG specific for kappa light chain) and 65 µL of ruthenium-labeled detection antibody were incubated with 10 µL of the samples for 4.5 minutes. Next, 60 µL streptavidin-coated magnetic beads binding to biotin were added to capture the antibody complex. Chemiluminescent emission signal was induced by a voltage in the measuring cell of the Elecsys® (Cobas, E411, Roche, Penzberg, Germany) leading to the oxidation of tripropylamine and ruthenium label. The ECL signal was detected by a photomultiplier at 620 nm.

For all animal groups (mAb, $F(ab')_2$ and Fab) examined with either FMT/CT and PET/MRI, linear functions of blood antibody levels were calculated based on the concentration levels determined by ECLIA. The time point x of the IC50 level (y=50) was determined.

Analysis of Anti-EGFR Expression and Anti-EGFR Antibody Binding

In order to confirm the in vivo EGFR expression of A-431 tumor cells and anti-EGFR antibody binding to EGFR receptors, fluorescence microscopy of tumors explanted of mice that were injected i.v. with labeled anti-EGFR constructs was performed. Tumor tissue sections of 1.5 µm thickness were scanned with a slide scanner (Pannoramic 250 Flash, 3D Histech, Budapest, HU) and binding of Alexa750-labeled anti-EGFR-constructs was investigated on a cellular level. In Supplemental Figure 1, a representative image is shown indicating a strong binding of anti-EGFR-mAb-Alexa750 to the cell surface of A-431 tumor cells.

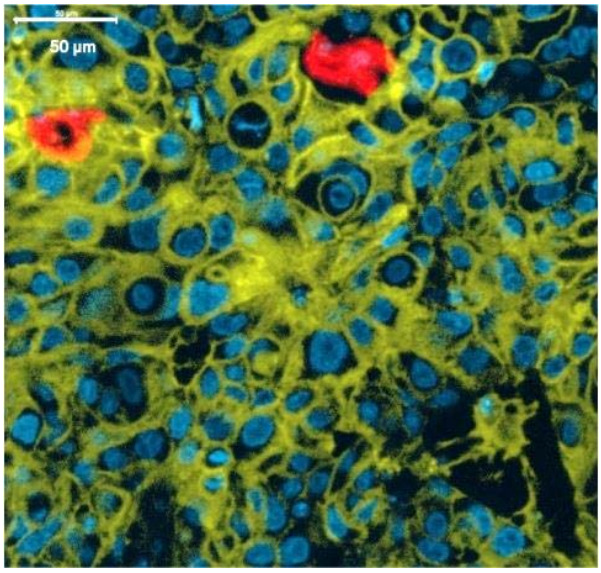

Supplemental Figure 1: Binding of anti-EGFR-mAb-Alexa750 to A-431 tumor cells 24 hours after injection. Representative section of the tumor showing strong binding of anti-EGFR-mAb-Alexa750 to A-431 tumor on a cellular level (blue = cell nuclei, yellow = anti-EFGR-mAb-Alexa750, red = vessel)."

(Supplements, page 3, lines 2-12).

Phantom Experiments with FMT/CT

Prior to the *in vivo* biodistribution study phantom experiments were performed in order to verify the reliability of the fluorescence quantification via FMT (Supplemental Figure 2). Phantoms, filled with 100 µl of Alexa750-labeled antibody (50 pmol), were placed subcutaneously (phantom 1) and into the mouse abdomen (phantoms 2, 3). The fluorescence signals of the phantoms were measured by FMT and quantified by FMT standard software (TrueQuant). In addition, the results of the FMT standard reconstruction were compared to the improved reconstruction using FMT/CT datasets and the algorithm considering absorption and scattering effects of the tissues [11]. The quantification via FMT standard reconstruction of fluorescent phantoms leads to an underestimation of the true values (see Supplemental Figure 2A). Furthermore, the reconstructed quantitative values of the phantoms placed in the abdomen (phantom 2 and 3) were strongly influenced by the position of the phantoms. The improved reconstruction of fused FMT/CT datasets, however, generated more reliable fluorescence quantitation (Phantom 1: 49 pmol, Phantom 2: 50 pmol, Phantom 3: 58 pmol) (see Supplemental Figure 2B).

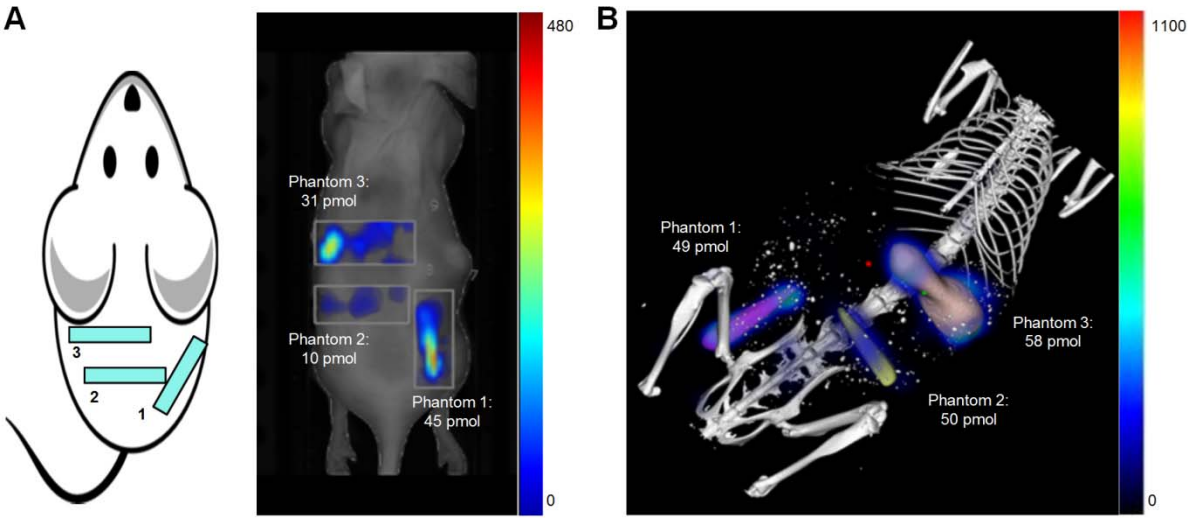

Supplemental Figure 2: Quantification of fluorescence phantoms placed in a mouse post-mortem. A Positions of three phantoms placed in a mouse and results of FMT measurement analyzed by FMT standard reconstruction. **B** Results of FMT/CT measurement analyzed by an improved reconstruction algorithm. The image shows a 3D overlay of the mouse bone structure with segmented phantom areas and fluorescence signals. The segmented phantoms are illustrated in pink, yellow and orange.

In Vivo Biodistribution after 2 h

Supplemental Table 1: Quantitative biodistribution values [Mean +/- SD in %ID/cm³] of anti -EGFR compounds (mAb, F(ab')$_2$, Fab) measured by FMT/CT and PET/MRI after two hours.

2 hours	FMT/CT			PET/MRI		
	mAb	F(ab')$_2$	Fab	mAb	F(ab')$_2$	Fab
Liver	34.4 +/- 9.4	40.1 +/- 6.5	32,1+/- 5.7	7.8 +/- 1.6	5.3 +/- 0.5	2.3 +/- 0.5
Kidneys	7.9 +/- 5.4	22.9 +/- 9.2	52.7 +/- 11.2	5,6 +/- 1	30.4 +/- 3.9	64.2 +/- 8.1
Muscle	2.8 +/- 2	2.3 +/- 2.9	1.5 +/- 1.8	0.9 +/- 0.2	0.6 +/- 0.2	0.4 +/- 0.4
Tumor	10.9 +/- 3.6	4.8 +/- 3	8.1 +/- 5.8	1.9 +/- 5.9	2.1 +/- 0.5	1.1 +/- 0.6

In Vivo Biodistribution after 24 h

In order to report the signal-to-noise ratio of the *in vivo* measurements, the tumor uptake-to-muscle ratio was calculated. This is shown for both *in vivo* imaging technologies.

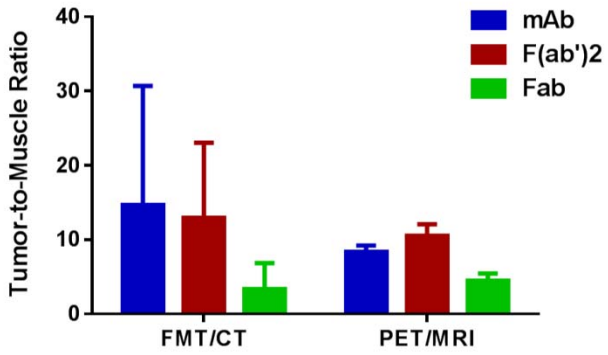

Supplemental Figure 3: Tumor-to-muscle ratio of %ID/cm³ values measured after 24 hours by FMT/CT or PET/MRI. The ratio of the quantitative values of tumor and muscle uptake of each mouse 24 hours after injection was determined and mean values for each group are shown in a bar chart.

Supplemental Table 2: Quantitative biodistribution values [Mean +/- SD in %ID/cm³] of anti-EGFR compounds (mAb, F(ab')$_2$, Fab) measured by FMT/CT and PET/MRI after 24 hours.

24 hours	FMT/CT			PET/MRI		
	mAb	F(ab')$_2$	Fab	mAb	F(ab')$_2$	Fab
Liver	20.9 +/- 2.5	21.3 +/- 4.5	7.5 +/- 3	5.4 +/- 0.5	3.6 +/- 0.5	3.5 +/- 0.4
Kidneys	3.9 +/- 1.3	7.8 +/- 4	7.1 +/- 3.6	3.5 +/- 0.3	21.1 +/- 1.4	24.3 +/- 1.6
Muscle	1.9 +/- 2.1	0.9 +/- 1.5	0.3 +/- 0.3	0.9 +/- 0.1	0.4 +/- 0.1	0.3 +/- 0.03
Tumor	13.1 +/- 2.5	3.7 +/- 1.7	1.9 +/- 1.9	7.3 +/- 1.2	3.7 +/- 0.7	1.2 +/- 0.16